ACS APPLIED MATERIALS & INTERFACES

www.acsami.org

Research Article

Electronic Packaging Enhancement Engineered by Reducing the Bonding Temperature via Modified Cure Cycles

Seong Yeon Park, Seung Yoon On, Junmo Kim, Jeonyoon Lee, Taek-Soo Kim, Brian L. Wardle,* and Seong Su Kim*

Cite This: *ACS Appl. Mater. Interfaces* 2023, 15, 11024−11032

Read Online

ACCESS | Metrics & More | Article Recommendations | Supporting Information

ABSTRACT: Semiconductor packaging continues to reduce in thickness following the overall thinning of electronic devices such as smartphones and tablets. As the package becomes thinner, the warpage of the semiconductor package becomes more important due to the reduced bending stiffness and driven by thermal residual stresses and thermal expansion mismatch during the epoxy molding compound (EMC) curing to create the package. To address this packaging reliability issue, in this study, we developed a modified cure cycle that adds a rapid cooling step to the conventional cure cycle (CCC) to enhance the reliability of the EMC molded to a copper substrate (EMC/Cu bi-layer package) by lowering the bonding temperature of the EMC/Cu bi-layer package. Modeling of the package via Timoshenko theory including effective cure shrinkage allowed the rapid cooling step to be quantified and confirmed via experiments. The modified cure cycle resulted in a 26% reduction in residual strain, a 27% reduction in curvature, and a 40% increase in peel strength compared to the CCC, suggesting that this is an effective new method for managing warping effects in such packaged structures.

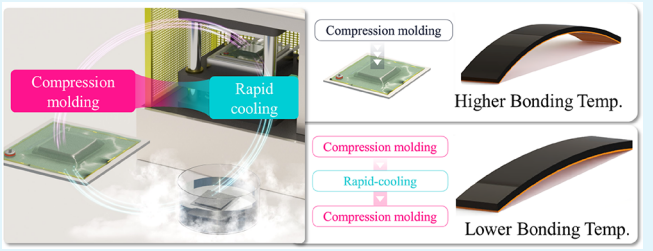

KEYWORDS: *semiconductor package, curvature, bonding temperature, cure shrinkage, cure cycle*

1. INTRODUCTION

Over the years, the thickness of electronic devices, such as smartphones and tablet PCs, has continually decreased according to consumer needs. As such, the semiconductor packages used in electronic devices are also being developed to be thinner and more highly integrated in performance.[1−3] Accordingly, various packages, such as system in package (SiP), package on package (PoP), and multi-chip package (MCP), have been developed.[4,5] One of the important roles of the semiconductor package is to protect the silicon chips and wires from mechanical and thermal shocks by encapsulating them with plastic molding technology and to effectively dissipate the heat generated during chip driving. Semiconductor plastic encapsulation technology uses an epoxy molding compound (EMC), which is over 80 wt % silica filler content polymeric composite material consisting of silica, epoxy resin, hardener, and other additives.[6,7] EMC is liquified and injected into the cavity with a plunger or placed directly into the cavity and liquified before the workpiece is immersed in it for resin molding and then cured by the manufacturer's recommended cure cycles. During the curing process, bonding occurs between EMC and the lead frame or substrate, and thermal residual stress is generated by the coefficient of thermal expansion (CTE) mismatch of the materials in the semiconductor package. As the package becomes thinner, warpage of the semiconductor package occurs due to the reduced bending stiffness via the area moment of inertia, caused by the thermal residual stresses. This warpage can not only damage a thin silicon chip but also cause a crack in the package and delamination of the package/chip interface, which has detrimental effects on the reliability of semiconductor packages. In addition, the possibility of cracking the solder joint between the package and motherboard increases, which lowers the semiconductor production yield.[8−13]

Recently, many studies have been conducted to reduce the warpage of semiconductor packages. Hong et al. analyzed the warpage according to the material properties of EMC: the lower the modulus and CTE and the higher the glass transition temperature (T_g) of EMC, the less the warpage.[14] Arayama et al. introduced a complex index termed "molding stress index" by multiplying the CTE by the storage modulus and found that EMC properties of the high-molding stress index are effective in mitigating the warpage of the ultrathin flip chip−chip scale package.[15] In addition, warpage analysis according to semiconductor package design, such as package geometries and

Received: November 25, 2022
Accepted: January 11, 2023
Published: January 25, 2023

sizes, has also been conducted. Yeon et al. analyzed the warpage according to the gap between silicon chips in wafer-level packaging. In addition, they analyzed the effect on the silicon chip movement.[16] Su et al. analyzed the warpage of the thickness and area ratio of the Si chip/EMC mold in a panel-level package.[17] However, this trial-error analysis is both cost and time-consuming because the warpage tendency varies according to the material properties, package size, and geometries. Therefore, studies on reducing the thermal residual stress have also been conducted by controlling the cure cycle. Chiu et al. analyzed the reduction of warpage by stress relaxation of the thermal residual stress generated during the curing process of EMC as the cure time in the cure cycle increases.[18] Sriwithoon et al. also analyzed the warpage according to the cure temperature.[19] However, the increase in the processing time results in an increase in production costs. In addition to increasing the cure cycle time, Kim et al. developed a smart cure cycle comprising a cooling and reheating process to improve the mechanical strength and fatigue life by reducing the thermal residual stress in the co-cured steel/carbon epoxy composite structures by lowering the bonding temperature. They also proceeded with the cooling process according to the degree of cure measured using a dielectric sensor.[20−22] However, previous studies controlling the curing process did not closely analyze the bonding temperature between the two materials, which principally drives the amount of warpage. The bonding temperature between dissimilar materials is generally obtained by measuring the curvature of the deformed bonding material and then calculating the bonding temperature using Timoshenko theory.[23] Since the curing process of epoxy is accompanied by cure shrinkage, which also affects the curvature, cure shrinkage must be also considered to determine the bonding temperature.

In this study, we developed a modified cure cycle that adds a rapid cooling step to the conventional cure cycle (CCC) to enhance the reliability of the EMC molded to a copper substrate (EMC/Cu bi-layer package) by lowering the bonding temperature of the EMC/Cu bi-layer package. In order to perform the rapid cooling shortly before the bonding temperature, Timoshenko theory considering the cure shrinkage was derived, and the theoretical bonding temperature was calculated by using the derived equation. Furthermore, the theoretical bonding temperature was verified through a novel experimental method to measure the interfacial strain. The additional rapid cooling setpoints were also set based on several rheological-based points, such as the lowest viscosity, to compare the effect of rapid cooling setpoints. The internal strain, peel strength, and curvature of the EMC/Cu bi-layer package were measured with respect to the rapid cooling setpoints to verify the reliability. Finally, the modulus and degree of cure of the EMC were measured to investigate the effect of the EMC with respect to rapid cooling setpoints.

2. EXPERIMENTAL SECTION

2.1. Cure Cycles of EMC/Cu Bi-layer Package. The EMC/Cu bi-layer package shown in Figure S1a was prepared in the form of a strip to analyze the warpage according to the EMC curing process. The Cu substrate (ILJIN, Korea) was immersed in acetic acid for 10 min to remove the oxide layer.[24]Figure 1 shows the experimental procedure for specimen preparation according to the curing cycle and its effect on the bonding temperature and curvature of the EMC/Cu bilayer package. The EMC/Cu bi-layer package was prepared by vacuum-assisted compression molding using a hot press (QM900A, QMESYS, Republic of Korea) after uniformly distributing the EMC on the Cu substrate. CCC suggested by the EMC manufacturer comprised a temperature ramp at a uniform rate of 10 °C/min from room temperature to 175 °C and a pressure of 4 MPa during the ramp. The bi-layer specimen was then cured at 175 °C for 2 h.

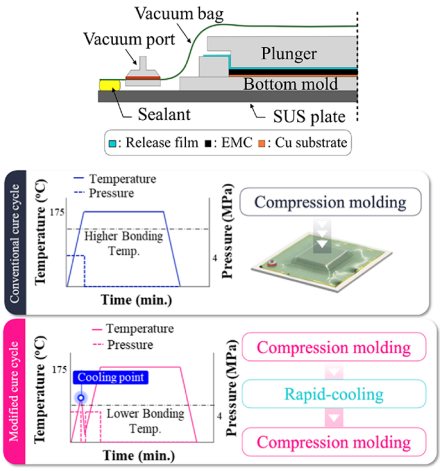

Figure 1. Experimental procedure and bonding temperature with respect to cure cycle.

In the designed modified cure cycle (explained below) with cooling and reheating, the same temperature ramp was applied until a specific temperature for rapid cooling was reached. Thereafter, the specimen was cooled rapidly to room temperature by dipping it into liquefied nitrogen to suppress the curing reaction and maintain EMC's degree of cure. Subsequently, the specimen was reheated to the cure temperature and cured under the same conditions as the CCC. In the reheating process, the degree of cure increases again and reaches a fully cured state with a lower bonding temperature, which results in lower curvature by reducing the CTE mismatch-induced length difference between EMC and Cu layers. In our modified cure cycle, a pressure of 4 MPa was applied only during the ramp. The specific temperature for rapid cooling was determined based on the bonding temperature of the EMC/Cu bi-layer package in the CCC.

2.2. Mechanical and Rheological Properties of EMC. Before analyzing the curvature of the EMC/Cu bi-layer package, EMC's elastic modulus and CTE affecting the curvature were measured using three dimensional-digital image correlation (3D-DIC) and a thermomechanical analyzer (TMA), respectively.[25,26]

In the case of the elastic modulus, the dimensions of specimens and testing conditions were in accordance with ASTM D47642.[27] The dimension of the specimen was set to 70 × 10 × 1 mm^3 in length, width, and thickness, respectively. The test was performed at a universal testing machine (INSTRON 5965, USA) with a gage length of 20 mm, a grip distance of 35 mm, and a loading velocity of 5 μm/s. The surface of EMC was sprayed with white ceramic patterns to track changes using the DIC method (ARAMIS, GOM, Germany). 3D-DIC cameras with a resolution of 4096 × 3000 were calibrated with a camera angle of 23.9°, and the distance between the camera and the specimen was set to 450 mm. The elastic modulus of EMC was measured with respect to the rapid cooling setpoint at room temperature. The CTE of the EMC specimen was measured using TMA. The size of the specimen was set to 20 mm × 5 mm × 1 mm for the expansion mode of TMA (TMA 402 F1, NETZSCH, Germany). The temperature was raised by 5 °C/min from 20 to 250 °C to measure the dimensional change of the specimen. The details of the results are shown in Figure S2 and Table 1.

A rheometer and a dielectric sensor were used to analyze the rheological properties of the EMC, such as the cure starts, the lowest viscosity, gelation, and solidification during the CCC. The cure state (cure start and cure end) of EMC was analyzed using an interdigital

https://doi.org/10.1021/acsami.2c21229
ACS Appl. Mater. Interfaces 2023, 15, 11024−11032

Table 1. Coefficient of Thermal Expansion of the Cured EMC at CCC

	EMC (T_g = 145 °C)	Cu
Elastic modulus (GPa)	30.72 (25 °C); 1.85 (150 °C)	110
CTE (10^{-6}/°C)	8.2 (<T_g); 26.5 (>T_g)	17

dielectric sensor. The interdigital dielectric sensor (Lacomtech, Republic of Korea) measures a dissipation factor, which is the ratio of the energy loss by the mobility of dipoles and ions in the EMC according to the direction of the alternating field, and the dissipation factor is related to the cure state.[28,29] In this study, the dissipation factor, D, was obtained in the EMC material using a commercial LCR meter (U1733C, Agilent, USA), which utilized an alternating current at 1 kHz frequency. As shown in Figure S1b, the interdigital dielectric sensor and K-type thermocouple were attached side by side to the center of the Cu substrate and embedded in the center of the EMC. The EMC was cured in the CCC to measure the cure start point of the EMC. The viscoelastic properties of the EMC were measured using a plate-type rheometer (HAAKE MARS, Thermo Fisher Scientific, USA). For viscosity measurements in the CCC, the EMC specimen had a diameter of 20 mm and thickness of 1 mm. When the upper plate was oscillating in a constant range of 1° and constant frequency of 1 Hz, the viscosity, storage, and loss modulus data of the EMC were obtained. From these data, the lowest viscosity, gelation, and solidification point of the EMC were found. The lowest viscosity indicates the point at which the viscosity reaches the lowest value, the gelation indicates the intersection of the storage and loss modulus, and the solidification is the point at which the viscosity reaches the maximum value after the gelation.[30,31] The details of the results are shown in Figure S3.

2.3. Effective Cure Shrinkage (ECS) of the EMC. In cure shrinkage, the distance between the molecules is reduced by cross-linking during curing, resulting in a volume reduction of the EMC. Cure shrinkage occurs at the same time as the cure starts; however, after gelation of the EMC, a transition from a liquid to a solid state occurs, and the mechanical strength (i.e., modulus) of the EMC is developed.[32,33] Therefore, as the warpage of the EMC/Cu bi-layer package was affected by cure shrinkage after gelation, which is called effective cure shrinkage (ECS), the ECS of EMC can be measured to calculate the bonding temperature.[32,34] To measure the ECS, the uncured EMC was sandwiched between the two silicon slides as shown in Figure S4, and the sizes of the uncured EMC specimen and Si cover were set to 5 mm × 5 mm × 0.07 mm and 10 mm × 10 mm × 0.2 mm, respectively. The Si cover prevents EMC from sticking to the sensing probe during curing and ensures uniform pressure on the EMC. The ECS of the EMC was measured in the CCC using TMA. The load was set to the minimum value of 0.001 N, at which no resin flow was caused by pressure.[35,36] The ECS was determined by the dimension change in the gelation temperature according to the following equation:

$$\varepsilon_{ECS} = \frac{H_{\text{Gelation curing}} - H_{\text{Gelation cured}}}{H_{\text{Gelation curing}}} \quad (1)$$

where ε_{ECS} is the ECS of the EMC, $H_{\text{Gelation curing}}$ is the initial thickness at gelation in the curing process, and $H_{\text{Gelation cured}}$ is the thickness at gelation after curing. The calculated ε_{ECS} represents isotropic ECS because EMC is a randomly distributed silica (spherical shape) reinforced epoxy composite material.

2.4. Curvature and Bonding Temperature of the EMC/Cu Bi-layer Package. The curvature of the EMC/Cu bi-layer package was measured according to temperature using 3D-DIC (ARAMIS, GOM, Germany).[37] The EMC/Cu bi-layer package was sprayed with a white ceramic pattern for tracking patterns using the DIC method in the same way as the modulus measurement.

During the cure cycle, bonding between EMC and Cu occurs at a temperature higher than room temperature. When the EMC/Cu bi-layer package is cooled to room temperature after the cure cycle is completed, residual stress is generated owing to the ECS of the EMC and CTE mismatch between the EMC and Cu, which results in curvature of the EMC/Cu bi-layer package. As shown in Figure 2,

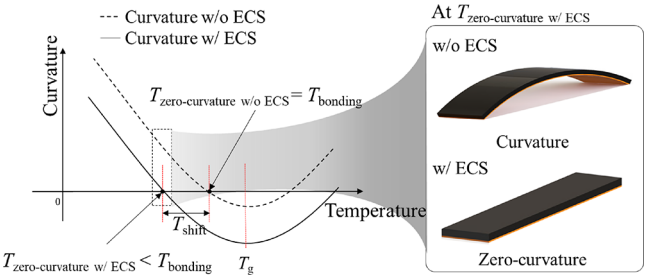

Figure 2. Curvature of the EMC/Cu bi-layer package w/o and w/ effective cure shrinkage (ECS).

when the temperature increases again, the curvature induced by CTE mismatch and EMC's ECS decreases to zero at a specific temperature, and this temperature is defined as zero-curvature temperature with ECS ($T_{\text{zero – curvature w/ECS}}$). In this case, $T_{\text{zero – curvature w/ECS}}$ has a lower than bonding temperature (T_{bonding}) because ECS only affects the curvature, not the bonding phenomenon between the two materials. When ECS is not considered, the zero-curvature temperature ($T_{\text{zero – curvature w/o ECS}}$) corresponds to T_{bonding} since the curvature is only determined by CTE mismatch-induced residual stress. Accordingly, when ECS is considered, the zero-curvature temperature is shifted to a lower value because the curvature is additionally affected by the permanent residual stress resulting from ECS.[38] Therefore, in order to proceed with rapid cooling shortly before the bonding temperature of the EMC/Cu bi-layer package, the bonding temperature using Timoshenko theory considering ECS of the EMC was calculated as follows:[23,38]

$$T_{\text{zero-curvature w/ECS}} - T = \frac{1}{\alpha_2 - \alpha_1}\left[\frac{k\left[h\left(3(1+m)^2 + (1+mn)\left(m^2 + \frac{1}{mn}\right)\right)\right]}{6(1+m)^2} - \varepsilon_{ECS}\right] \quad (2)$$

$$T_{\text{shift}} = \frac{\varepsilon_{ECS}}{\alpha_2 - \alpha_{\text{average\_1}}} \quad (3)$$

$$T_{\text{bonding}} = T_{\text{zero-curvature w/ECS}} + T_{\text{shift}} \quad (4)$$

where k is the curvature of the EMC/Cu bi-layer package, material 1 and 2 are the EMC and Cu, m is the thickness ratio of the EMC to the Cu (h_1/h_2), n is the modulus of the EMC to the Cu (E_1/E_2), h is the total thickness of the EMC/Cu bi-layer package ($h_1 + h_2$), ε_{ECS} is the effective cure shrinkage, and α_1, $\alpha_{\text{average\_1}}$, α_2 are the CTE (before T_g) and average CTE of EMC and CTE of Cu, respectively. The detailed derivation of the equation is presented in the Supporting Information (Figures S5 and S6, eqs S1−S15).

2.5. Interfacial and Internal Strain of the EMC/Cu Bi-layer Package. To verify the analytical bonding temperature considering the ECS in the CCC, the interfacial strain between the EMC and Cu was measured using a Fiber Bragg Grating (FBG) sensor.[39−41] For the measurement of the interfacial strain, the dimensions of the specimen were the same as those of the EMC/Cu bi-layer package. The FBG sensor was attached to the center of the Cu substrate, and the EMC was stacked on it to measure the strain of EMC close to the interface between the two materials, as shown in Figure 3a. In addition, an FBG sensor and a thermocouple were attached to the center of the Cu substrate, as shown in Figure 3b, to measure the strain of the Cu

https://doi.org/10.1021/acsami.2c21229
ACS Appl. Mater. Interfaces 2023, 15, 11024−11032

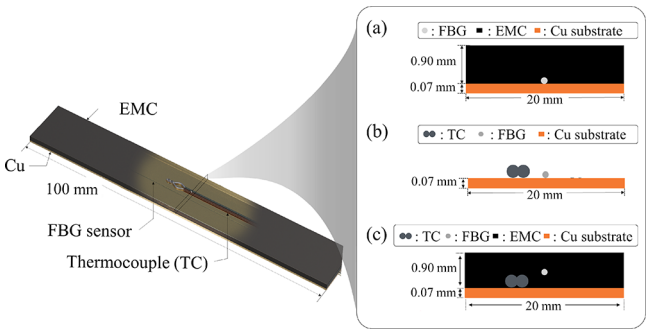

Figure 3. Measurement of the interfacial strain of the EMC/Cu bi-layer package using the FBG sensor; (a) strain of EMC close to the interface between EMC and Cu, (b) strain of Cu, (c) and internal strain of the EMC/Cu bi-layer package.

substrate. The interfacial strain between EMC and Cu was analyzed by subtracting the strain of the Cu substrate from the strain of EMC close to the interface to exclude the effect of the Cu expansion. In addition, the internal strain of the EMC/Cu bi-layer package specimen was measured to compare the thermal residual internal strain with respect to the rapid cooling setpoint by embedding an FBG sensor and a thermocouple within the EMC layer, as shown in Figure 3c. The polyimide-coated single-mode FBG (Fiberpro, Republic of Korea) sensor was used. The wavelength, grating reflectivity, and gauge length of the FBG sensor were 1550 nm, >90%, and 10 mm, respectively.

2.6. Measurement of the Peel Strength of the EMC/Cu Bi-layer Package Using a 90° Peel Test. A 90° peel test was performed to measure the peel strength of the EMC/Cu bi-layer package with respect to the rapid cooling setpoint.[42] The dimensions of the specimens and testing conditions were based on D6862-11.[43] The peel tests were carried out with an MTS 600 mechanical testing machine using a 20 N load cell with a 90° peeling angle. The Cu substrate was fixed to a 90° jig, and the EMC was fixed to the pull-off table. The displacement was applied to the jig in the upward direction and the pull-off table in the right direction, and the displacement speed was set at 0.1 mm/s. The peel strength was calculated by dividing the average load by the width of the specimen, as follows:

$$\text{average peel strength}\left(\frac{\text{N}}{\text{m}}\right) = \frac{\text{average load (N)}}{\text{bond width (m)}} \quad (5)$$

2.7. Degree of Cure of EMC. The differential scanning calorimetry (DSC) method was used to analyze the degree of cure of the EMC with respect to the rapid cooling setpoint. Small samples of 9−11 mg of the EMC were used for DSC (Q20, TA Instruments, USA) measurements under dynamic scanning.[28] A dynamic DSC run was performed by scanning the heat flow from room temperature to 250 °C at 1, 2, 5, and 10 °C/min to measure the total heat generation. The average of the total heat generation according to the ramp was used to calculate the degree of cure. The degree of cure was estimated by comparing the area of the exothermic peak observed in the DSC curve of the EMC during heat processing. To analyze the EMC degree of cure with respect to the rapid cooling setpoint using the total heat generation, the residual heat generation of the cured EMC was measured by increasing the temperature from room temperature to 250 °C at 5 °C/min.

3. RESULTS AND DISCUSSION

3.1. Bonding Temperature of the EMC/Cu Bi-layer Package. Figure 4a shows the thickness change of the EMC in CCC measured by TMA to analyze the ECS of the EMC. The average ECS was approximately 0.02%, according to eq 1, which is similar to values in the other works dealing with cure shrinkage of EMC.[44,45] Figure S1c shows the actual EMC/Cu bi-layer package fabricated in the CCC, and the curvature in the convex form appears at room temperature. Figure 4b shows the measured curvature of the EMC/Cu bi-layer package fabricated in CCC according to temperature and the comparison of zero-curvature and bonding temperature of the EMC/Cu bi-layer package from Timoshenko theory w/o and w/ ECS, and the experimental results are summarized in Figure 5

The curvature occurred in a convex form until the zero-curvature temperature because the CTE of the Cu was larger than that of the EMC, and the zero-curvature of the EMC/Cu bi-layer package appeared at approximately 107.5 °C. The analytical zero-curvature temperature of the EMC/Cu bi-layer package based on eq 2 considering the ECS (w/ ECS) was 109.8 °C, which is similar to the measured temperature. Using the analytical zero-curvature temperature, the analytical bonding temperature of the EMC/Cu bi-layer package was calculated as 145.8 °C according to eqs 3 and 4. On the other hand, when Timoshenko theory was applied without considering the ECS (w/o ECS), the analytical bonding temperature was 132.6 °C, which is the same as the analytical zero-curvature temperature because there is no T_{shift}. Figure 6 shows the interfacial strain profile between the EMC and Cu layer in CCC measured using an FBG sensor to confirm the bonding temperature of the EMC/Cu bi-layer package. There

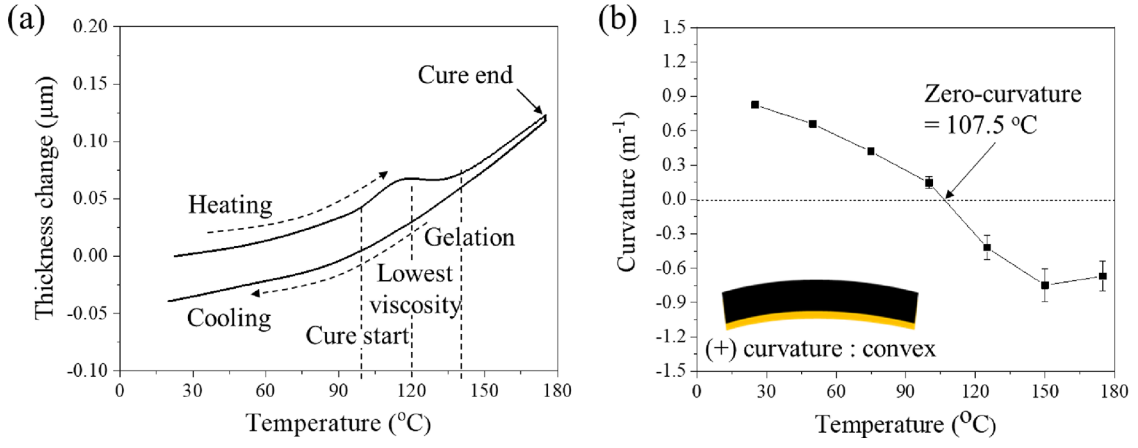

Figure 4. Analysis of chemical shrinkage and warpage using the conventional cure cycle (CCC); (a) thickness change of EMC, (b) curvature of EMC/Cu bi-layer package manufactured.

https://doi.org/10.1021/acsami.2c21229
ACS Appl. Mater. Interfaces 2023, 15, 11024−11032

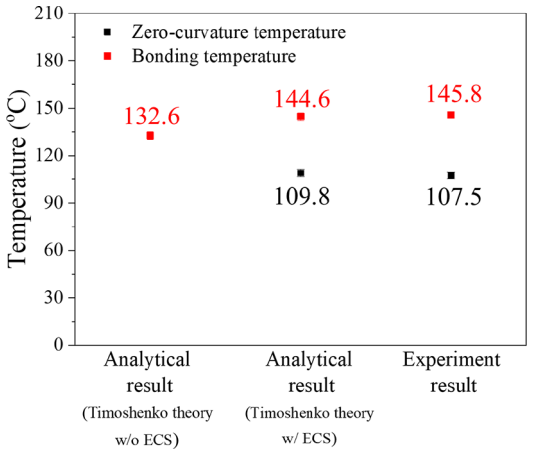

Figure 5. Comparison of zero-curvature and bonding temperature of the EMC/Cu bi-layer package from Timoshenko theory w/o and w/ ECS and experimental results of the specimen fabricated in CCC.

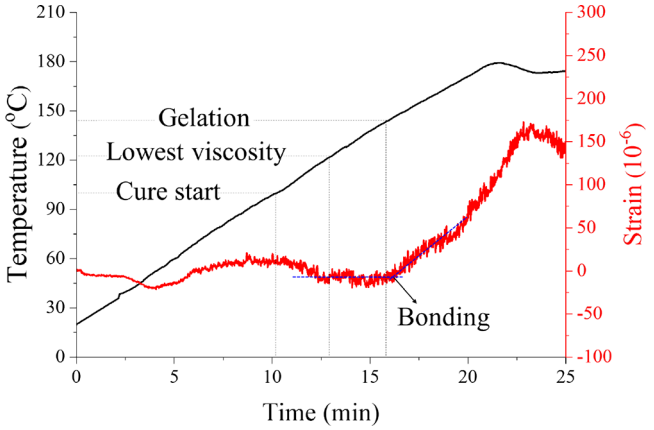

Figure 6. Interfacial strain of EMC and Cu in the conventional cure cycle.

was no change in the interfacial strain as the temperature increased up to the gelation point, indicating that the bonding of EMC and Cu did not occur. Accordingly, the intersection point of the trend line before and after the increase in interfacial strain is expressed as the bonding temperature, which is 145.8 °C, almost the same as the analytical bonding temperature (144.6 °C) of the EMC/Cu bi-layer package. From this result, it can be confirmed that the ECS should be considered to determine the bonding temperature based on Timoshenko theory. In addition, Figure S7 shows the curvature and bonding temperature of the EMC/Cu bi-layer package fabricated in the CCC with respect to EMC's thickness. The curvature decreased as the EMC's thickness increased, but in the analytical bonding temperature, no significant change was observed with respect to the EMC's thickness. This is because the rheological property changes of EMC are identical within the same cure cycle.[46]

Considering the previous results, the rapid cooling shortly before the bonding temperature in the CCC may significantly affect the lowering of the bonding temperature between the EMC and Cu in the modified cure cycle.[20] Accordingly, to investigate the effect of rapid cooling on the bonding temperature, rapid cooling was performed at 100 °C (near the cure start), 120 °C (near the temperature showing the lowest viscosity), 140 °C (shortly before the actual bonding temperature), and 160 °C (near the solidification temperature).

3.2. Curvature, Bonding Temperature, Modulus, and Degree of Cure of the EMC/Cu Bi-layer Package with Respect to the Rapid Cooling Setpoint. Figure S8 shows the curvature changes according to the temperature of the EMC/Cu bi-layer package specimens fabricated at various cooling setpoints. The curvature and zero-curvature temperature of the specimens fabricated in the modified cure cycles were reduced compared to the CCC regardless of the rapid cooling setpoint. Figure S9 shows the comparison between the analytical zero-curvature temperature considering the ECS and the measured zero-curvature temperature with respect to the cooling setpoint, and it can be seen that the two results are very similar. Figure 7a shows the measured curvature at room temperature and the analytical bonding temperature of the EMC/Cu bi-layer package with and without consideration of ECS with respect to cure cycles. The analytical bonding temperature without consideration of the ECS was substantially lower than that with consideration of the ECS with respect to the rapid cooling setpoint.

The curvature and analytical bonding temperature w/ ECS of EMC/Cu bi-layer package fabricated with a rapid cooling setpoint of 140 °C, just before the bonding temperature (144.6 °C) of the CCC considering ECS, was significantly reduced by

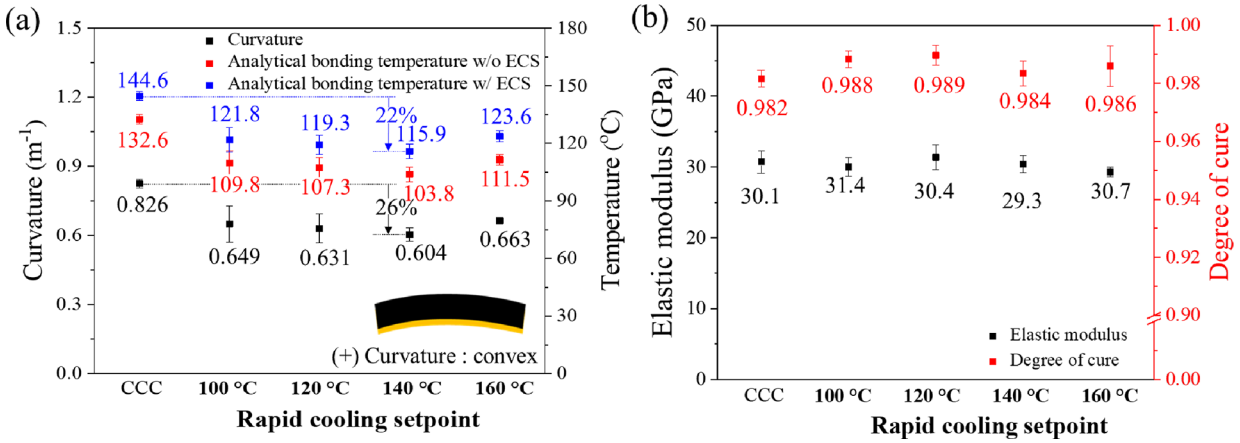

Figure 7. Mechanical behavior of the EMC/Cu bi-layer package with respect to the rapid cooling setpoint; (a) measured curvature and analytical bonding temperature w/o and w/ ECS, (b) modulus and degree of cure of the EMC with respect to the rapid cooling setpoint.

https://doi.org/10.1021/acsami.2c21229
ACS Appl. Mater. Interfaces 2023, 15, 11024−11032

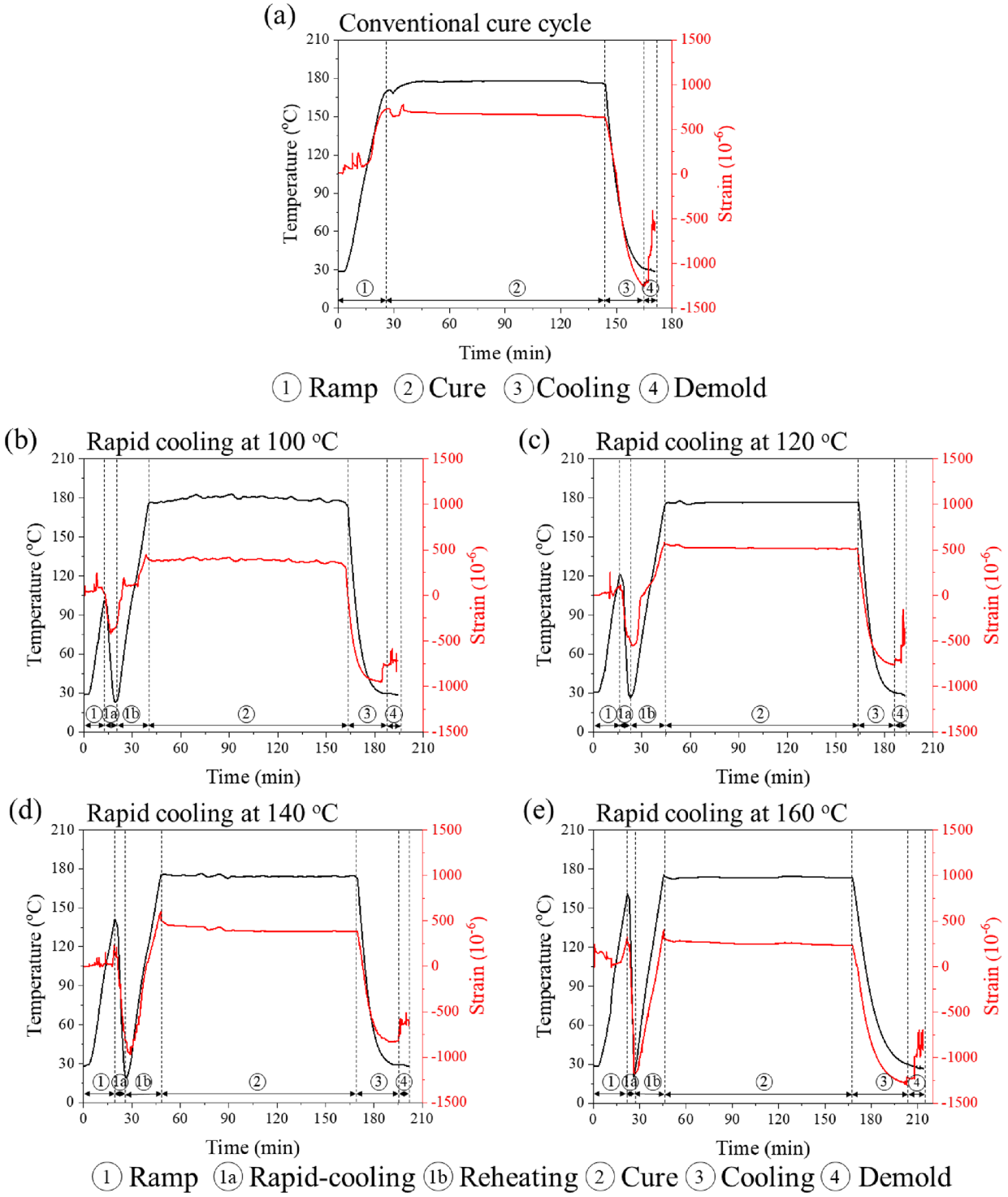

Figure 8. Internal strain profile of the EMC/Cu bi-layer package during the cure cycle with respect to rapid cooling setpoint: (a) CCC, (b) rapid cooling at 100 °C, (c) rapid cooling at 120 °C, (d) rapid cooling at 140 °C, and (e) rapid cooling at 160 °C.

26% and 22% compared to those fabricated with CCC. From these results, it can be confirmed once again that ECS must be considered in order to determine a rapid cooling setpoint to reduce curvature. Figure 7b shows the EMC modulus and the degree of cure with respect to cure cycles. The EMC modulus and degree of curing applied with the modified cooling cycles were almost similar to those applied with the CCC, which means that rapid cooling did not affect the EMC modulus and degree of cure.

3.3. Residual Internal Strain and Peel Strength of the EMC/Cu Bi-layer Package with Respect to the Rapid Cooling Setpoint. Figure 8 shows the internal strain profile during the cure cycle measured by the FBG sensor with respect to the rapid cooling setpoint. The CCC was divided into four regions according to the steps to analyze the internal strain profiles, as shown in Figure 8a. Region 1 (Ramp) shows the heating process from room temperature to 175 °C. In this region, the tensile strain was generated by the applied pressure

https://doi.org/10.1021/acsami.2c21229
ACS Appl. Mater. Interfaces 2023, 15, 11024−11032

and positive CTE of the EMC and Cu. Region 2 (Cure) shows the isothermal dwelling process at 175 °C for 2 h without pressure. In this region, the strain gradually decreased slightly owing to stress relaxation. Region 3 (Cooling) shows the cooling process from 175 °C to room temperature, and the strain was reduced. Region 4 (Demold) shows the demold process of the EMC/Cu bi-layer package specimen from the mold. After demold, the strain change occurred due to the curvature.

The modified cure cycle with respect to the rapid cooling setpoint was divided into six regions according to the steps, as shown in Figure 8b–e. In Region 1 (Ramp), the internal strain change was similar to that of CCC. Region 1a (Rapid cooling) shows the strain change that occurred during the rapid cooling. The compressive strain was mainly generated by thermal contraction during the rapid cooling. In Regions 1b to 4, a profile similar to that of CCC was observed. The thermal residual internal strains of each cure cycle were calculated by subtracting the strain at the demold region from the average strain in the cure region. Figure 9 represents the residual

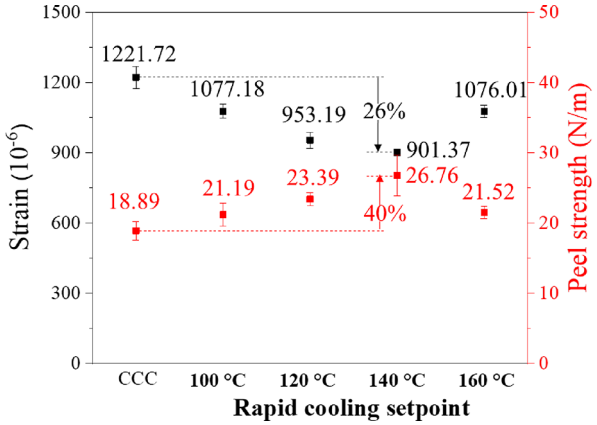

Figure 9. Residual internal strain and peel strength of the EMC/Cu bi-layer package with respect to the rapid cooling setpoint.

internal strains and peel strength of the EMC/Cu bi-layer package with respect to the rapid cooling setpoint. Similar to the trend in the curvature results, the residual internal strain of the modified cure cycle decreased regardless of the rapid cooling setpoint. The specimen fabricated in a modified cure cycle with rapid cooling at 140 °C showed the lowest residual strain, which was reduced by 26% compared to the specimen fabricated in the CCC. The peel strength of the EMC/Cu bi-layer package showed a similar tendency to that of the residual internal strain. The peel strength of the specimen in a modified cure cycle with rapid cooling at 140 °C increased by approximately 40% compared to that of the specimen fabricated in the CCC. Consequently, it was confirmed that the reduction of the bonding temperature led to reduced curvature, reduced residual internal strain, and improved peel strength of the EMC/Cu bi-layer package.

4. CONCLUSIONS

In this study, we applied modified cure cycles with rapid cooling to enhance the reliability of the EMC/Cu bi-layer package. The effects of the rapid cooling were investigated by measuring the bonding temperature, residual strain, peel strength, and curvature. Based on these results, the following conclusions were drawn:

1) The analytical bonding temperature considering the cure shrinkage of the EMC was calculated by measuring the curvature of the EMC/Cu bi-layer package fabricated by the CCC and verified through the interfacial strain measurement of EMC and Cu using the FBG sensor.
2) When the specimen was rapidly cooled before the experimentally-determined bonding temperature for the CCC, the residual internal strain and curvature decreased by 26% and 27%, respectively, and the peel strength increased by 40% compared to the specimen fabricated in the CCC.
3) The modulus and degree of cure of the EMC were constant regardless of the cure cycles.
4) The reduction in residual strain and curvature and the improvement in peel strength are attributed to the reduced bonding temperature of the EMC/Cu bi-layer package fabricated in the modified cure cycle.

From these results, it should be noted that the exact prediction of the bonding temperature considering the effective cure shrinkage makes it possible to find the optimum cooling setpoint and consequently enhance the reliability of the EMC/Cu bi-layer package. For future works, a rapid heating and cooling device using carbon nanotubes will be applied to the modified cure cycle to replace the rapid cooling using liquified nitrogen.

ASSOCIATED CONTENT

Supporting Information

The Supporting Information is available free of charge at https://pubs.acs.org/doi/10.1021/acsami.2c21229.

Schematic diagram of the specimen; mechanical properties of the EMC as a function of temperature; rheological analysis result; schematic of cure shrinkage measurement setup; curvature of the EMC/Cu bi-layer package fabricated with respect to the rapid cooling setpoint; analytical and experimental zero-curvature temperature with respect to the rapid cooling setpoint (PDF)

AUTHOR INFORMATION

Corresponding Authors

Brian L. Wardle − *Department of Aeronautics and Astronautics and Department of Mechanical Engineering, Massachusetts Institute of Technology, Cambridge, Massachusetts 02139, United States;* orcid.org/0000-0003-3530-5819; Email: wardle@mit.edu

Seong Su Kim − *Department of Mechanical Engineering, Korea Advanced Institute of Science and Technology (KAIST), Daejeon 305-701, Republic of Korea;* orcid.org/0000-0001-8722-0505; Email: seongsukim@kaist.ac.kr

Authors

Seong Yeon Park − *Department of Mechanical Engineering, Korea Advanced Institute of Science and Technology (KAIST), Daejeon 305-701, Republic of Korea*

Seung Yoon On − *Department of Mechanical Engineering, Korea Advanced Institute of Science and Technology (KAIST), Daejeon 305-701, Republic of Korea*

Junmo Kim − *Department of Mechanical Engineering, Korea Advanced Institute of Science and Technology (KAIST), Daejeon 305-701, Republic of Korea*

https://doi.org/10.1021/acsami.2c21229
ACS Appl. Mater. Interfaces 2023, 15, 11024−11032

Jeonyoon Lee − *Department of Aerospace Engineering, Korea Advanced Institute of Science and Technology (KAIST), Daejeon 305-701, Republic of Korea;* orcid.org/0000-0003-4735-2153

Taek-Soo Kim − *Department of Mechanical Engineering, Korea Advanced Institute of Science and Technology (KAIST), Daejeon 305-701, Republic of Korea;* orcid.org/0000-0002-2825-7778

Complete contact information is available at: https://pubs.acs.org/10.1021/acsami.2c21229

Author Contributions

S.Y.P.: Conceptualization, methodology, data curation, writing − original draft preparation, and writing − reviewing and editing. S.Y.O.: Visualization. J.K.: Data curing. J.L.: Methodology. B.L.W.: Writing − reviewing and editing. S.S.K.: Supervising and writing − reviewing and editing.

Notes

The authors declare no competing financial interest.

■ ACKNOWLEDGMENTS

This work was supported by the National Research Foundation of Korea (NRF) grant funded by the Korea government (MSIT) (No. 2020R1A2C201096512) and also supported by the BK21 FOUR Program of the National Research Foundation Korea (NRF) grant funded by the Ministry of Education (MOE).

■ ABBREVIATIONS

EMC, epoxy molding compound
CCC, conventional cure cycle
EMC/Cu bi-layer package, EMC molded to a copper
SiP, system in package
MCP, multi-chip package
CTE, coefficient of thermal expansion
ECS, effective cure shrinkage.

■ REFERENCES

(1) Bohr, M. T.Logic technology scaling to continue moore's law. In *2018 IEEE 2nd Electron Devices Technology and Manufacturing Conference (EDTM)*; 2018; IEEE: pp. 1−3.

(2) Wu, T.; Tsukada, Y.; Chen, W.Materials and mechanics issues in flip-chip organic packaging. In *1996 Proceedings 46th Electronic Components and Technology Conference*; 1996; IEEE: pp. 524−534.

(3) Van Driel, W.; Zhang, G.; Janssen, J.; Ernst, L.; Su, F.; Chian, K.; Yi, S.Prediction and verification of process-induced thermal deformation of electronic packages using non-linear FEM and 3D interferometry. In *Proc. EuroSimE*; PCCL2002; Vol. *362*.

(4) Al-Sarawi, S. F.; Abbott, D.; Franzon, P. D. A review of 3-D packaging technology. *IEEE Trans. Compon., Packag., Manuf. Technol., Part B* **1998**, *21*, 2−14.

(5) Hong, J.; Choi, K.; Oh, D.; Park, S.; Shao, S.; Wang, H.; Niu, Y.Design guideline of 2.5 D package with emphasis on warpage control and thermal management. In *2018 IEEE 68th Electronic Components and Technology Conference (ECTC)*, 2018; IEEE: pp. 682−692.

(6) Kinjo, N.; Ogata, M.; Nishi, K.; Kaneda, A. Epoxy molding compounds as encapsulation materials for microelectronic devices. *Polym. Phys.* **1989**, 1−48.

(7) Komori, S.; Sakamoto, Y.Development trend of epoxy molding compound for encapsulating semiconductor chips. In *Materials for Advanced Packaging*; Springer, 2009; pp. 339−363, DOI: 10.1007/978-0-387-78219-5_10.

(8) Tsai, M.-Y.; Wang, C. T.; Hsu, C. H. The effect of epoxy molding compound on thermal/residual deformations and stresses in IC packages during manufacturing process. *IEEE Trans. Compon., Packag., Manuf. Technol., Part A* **2006**, *29*, 625−635.

(9) Sadeghinia, M.; Jansen, K. M. B.; Ernst, L. J. Characterization of the viscoelastic properties of an epoxy molding compound during cure. *Microelectron. Reliab.* **2012**, *52*, 1711−1718.

(10) Kim, Y. K.; Park, I. S.; Choi, J. Warpage mechanism analyses of strip panel type PBGA chip packaging. *Microelectron. Reliab.* **2010**, *50*, 398−406.

(11) Chae, M.; Ouyang, E.Strip warpage analysis of a flip chip package considering the mold compound processing parameters. In *2013 IEEE 63rd Electronic Components and Technology Conference*, 2013; IEEE: pp. 441−448.

(12) Liu, W.; Shi, F. G.Effect of the viscoelastic behavior of molding compounds on crack propagation in IC packages. In *52nd Electronic Components and Technology Conference 2002.(Cat. No. 02CH37345)*, 2002; IEEE: pp. 854−858.

(13) Yang, S. Y.; Kwon, W.-S.; Lee, S.-B. Chip warpage model for reliability prediction of delamination failures. *Microelectron. Reliab.* **2012**, *52*, 718−724.

(14) Hong, J.; Gao, S.; Park, S.; Moon, S.; Baek, J.; Choi, S.; Yi, S.Parametric design study for minimized warpage of WL-CSP. In *2008 2nd Electronics System-Integration Technology Conference*; 2008; IEEE: pp. 187−192.

(15) Arayama, C.; Akashi, T.; Tomita, Y.; Kanagawa, N.Method for Mitigating the Warpage of Ultra-Thin FC-CSPs by Controlling of EMC Properties. In *2019 IEEE 69th Electronic Components and Technology Conference (ECTC)*; 2019; IEEE: pp. 1022−1027.

(16) Yeon, S.; Park, J.; Lee, H.-J. Compensation method for die shift caused by flow drag force in wafer-level molding process. *Micromachines* **2016**, *7*, 95.

(17) Su, M.; Cao, L.; Lin, T.; Chen, F.; Li, J.; Chen, C.; Tian, G. Warpage simulation and experimental verification for 320 mm× 320 mm panel level fan-out packaging based on die-first process. *Microelectron. Reliab.* **2018**, *83*, 29−38.

(18) Chiu, T.-C.; Huang, H.-W.; Lai, Y.-S. Warpage evolution of overmolded ball grid array package during post-mold curing thermal process. *Microelectron. Reliab.* **2011**, *51*, 2263−2273.

(19) Sriwithoon, N.; Ugsornrat, K.; Srisuwitthanon, W.; Thonglor, P.Warpage of QFN package in post mold cure process of integrated circuit packaging. In *Journal of Physics: Conference Series*; 2017; IOP Publishing: Vol. *901*, p 012089.

(20) Kim, H. S.; Park, S. W.; Lee, D. G. Smart cure cycle with cooling and reheating for co-cure bonded steel/carbon epoxy composite hybrid structures for reducing thermal residual stress. *Composites, Part A* **2006**, *37*, 1708−1721.

(21) Kim, H. S.; Lee, D. G. Reduction of fabricational thermal residual stress of the hybrid co-cured structure using a dielectrometry. *Compos. Sci. Technol.* **2007**, *67*, 29−44.

(22) Kim, H.-S.; Yoo, S.-H.; Chang, S.-H. In situ monitoring of the strain evolution and curing reaction of composite laminates to reduce the thermal residual stress using FBG sensor and dielectrometry. *Composites, Part B* **2013**, *44*, 446−452.

(23) Timoshenko, S. Analysis of bi-metal thermostats. *Josa* **1925**, *11*, 233−255.

(24) Chavez, K. L.; Hess, D. W. A novel method of etching copper oxide using acetic acid. *J. Electrochem. Soc.* **2001**, *148*, G640.

(25) Lee, T.-I.; Kim, C.; Kim, M. S.; Kim, T.-S. Flexural and tensile moduli of flexible FR4 substrates. *Polym. Test.* **2016**, *53*, 70−76.

(26) Kavdir, E. Ç.; Aydin, M. D. The investigation of mechanical properties of a structural adhesive via digital image correlation (DIC) technic. *Composites, Part B* **2019**, *173*, 106995.

(27) "Standard Guide for Testing Polymer Matrix Composite Materials". *ASTM D4762*; ASTM International2011.

(28) Kim, J. S.; Lee, D. G. Measurement of the degree of cure of carbon fiber epoxy composite materials. *J. Compos. Mater.* **1996**, *30*, 1436−1457.

(29) Jung, K.-C.; Roh, I.-T.; Chang, S.-H. Evaluation of mechanical properties of polymer concretes for the rapid repair of runways. *Composites, Part B* **2014**, *58*, 352−360.
(30) Cadenato, A.; Salla, J.; Ramis, X.; Morancho, J. M.; Marroyo, L. M.; Martin, J. L. Determination of gel and vitrification times of thermoset curing process by means of TMA, DMTA and DSC techniques: TTT diagram. *J. Therm. Anal. Calorim.* **1997**, *49*, 269−279.
(31) Yuksel, O.; Sandberg, M.; Baran, I.; Ersoy, N.; Hattel, J. H.; Akkerman, R. Material characterization of a pultrusion specific and highly reactive polyurethane resin system: Elastic modulus, rheology, and reaction kinetics. *Composites, Part B* **2021**, *207*, 108543.
(32) Wang, Y.; Woodworth, L.; Han, B. Simultaneous measurement of effective chemical shrinkage and modulus evolutions during polymerization. *Exp. Mech.* **2011**, *51*, 1155−1169.
(33) Yu, H.; Mhaisalkar, S. G.; Wong, E. H. Effect of temperature on the cure shrinkage measurement of non-conductive adhesives for flip chip interconnects. *J. Mater. Res.* **2005**, *20*, 1324−1329.
(34) Yu, H.; Mhaisalkar, S. G.; Wong, E. H. Cure shrinkage measurement of nonconductive adhesives by means of a thermo-mechanical analyzer. *J. Electron. Mater.* **2005**, *34*, 1177−1182.
(35) Kwon, W.-S.; Paik, K.-W. Fundamental understanding of ACF conduction establishment with emphasis on the thermal and mechanical analysis. *Int. J. Adhes. Adhes.* **2004**, *24*, 135−142.
(36) Phansalkar, S. P.; Kim, C.; Han, B.; Gromala, P. J. Volumetric effective cure shrinkage measurement of dual curable adhesives by fiber Bragg grating sensor. *J. Mater. Sci.* **2020**, *55*, 9655−9664.
(37) Kim, C.; Lee, T.-I.; Kim, M.; Kim, T.-S. Warpage analysis of electroplated Cu films on fiber-reinforced polymer packaging substrates. *Polymer* **2015**, *7*, 985−1004.
(38) Zhu, W.; Li, G.; Sun, W.; Che, F.; Sun, A.; Wang, C.; Tan, H.; Zhao, B.; Chin, N.Cure shrinkage characterization and its implementation into correlation of warpage between simulation and measurement. In *2007 International Conference on Thermal, Mechanical and Multi-Physics Simulation Experiments in Microelectronics and Micro-Systems. EuroSime 2007*, 2007; IEEE: pp. 1−8.
(39) Kersey, A. D.; Davis, M. A.; Patrick, H. J.; LeBlanc, M.; Koo, K. P.; Askins, C. G.; Putnam, M. A.; Friebele, E. J. Fiber grating sensors. *J. Lightwave Technol.* **1997**, *15*, 1442−1463.
(40) Kuang, K. S. C.; Kenny, R.; Whelan, M. P.; Cantwell, W. J.; Chalker, P. R. Embedded fibre Bragg grating sensors in advanced composite materials. *Compos. Sci. Technol.* **2001**, *61*, 1379−1387.
(41) Mulle, M.; Collombet, F.; Olivier, P.; Grunevald, Y.-H. Assessment of cure residual strains through the thickness of carbon−epoxy laminates using FBGs, Part I: Elementary specimen. *Composites, Part A* **2009**, *40*, 94−104.
(42) Chen, Y.; Chen, Y.; Wang, J.; Zhu, K.; Jia, L.; Wang, S.; He, W.; Chen, Q.; Miao, H.; Zhou, J. Enhancing adhesion performance of sputtering Ti/Cu film on pretreated composite prepreg for stacking structure of IC substrates. *Composites, Part B* **2019**, *158*, 400−405.
(43) "Standard Test Method for 90 Degree Peel resistance of adhesives". *ASTM D6862−11*; ASTM International2021.
(44) Kim, C.; Phansalkar, S. P.; Lee, H. S.; Han, B. Measurement of effective cure shrinkage of epoxy−based molding compound by fiber Bragg grating sensor usingtwo−stagecuring process. *J. Appl. Polym. Sci.* **2022**, *139*, 51620.
(45) Oota, K.; Saka, M. Cure shrinkage analysis of epoxy molding compound. *Polym. Eng. Sci.* **2001**, *41*, 1373−1379.
(46) Dulude, C.; Hassan, M.; Ahmed, E. A.; Benmokrane, B. Punching shear behavior of flat slabs reinforced with glass fiber-reinforced polymer bars. *ACI Struct. J.* **2013**, *110*, 723.

https://doi.org/10.1021/acsami.2c21229
ACS Appl. Mater. Interfaces 2023, 15, 11024−11032